Title

Genetic properties underlying transcriptional variability across different perturbations

Author list

Saburo Tsuru[1,*] & Chikara Furusawa[1,2,3,*]

Affiliations

[1]Universal Biology Institute, Graduate School of Science, The University of Tokyo, 7-3-1 Hongo, Bunkyo-ku, Tokyo 113-0033, Japan

[2]Department of Physics, Graduate School of Science, The University of Tokyo, 7-3-1 Hongo, Bunkyo-ku, Tokyo 113-0033, Japan

[3]Center for Biosystems Dynamics Research (BDR), RIKEN, 6-2-3 Furuedai, Suita, Osaka 565-0874, Japan

*Corresponding authors:

Saburo Tsuru

E-mail: saburotsuru@gmail.com

Chikara Furusawa

chikara.furusawa@riken.jp

Abstract

The rate and direction of phenotypic evolution depend on the availability of phenotypic variants induced genetically or environmentally. It is widely accepted that organisms do not display uniform phenotypic variation, with certain variants arising more frequently than others in response to genetic or environmental perturbations. Previous studies have suggested that gene regulatory networks channel both environmental and genetic influences. However, how the gene regulatory networks influence phenotypic variation remains unclear. To address this, we characterize transcriptional variations in *Escherichia coli* under environmental and genetic perturbations. Based on the current understanding of transcriptional regulatory networks, we identify genetic properties that explain gene-to-gene differences in transcriptional variation. Our findings highlight the role of gene regulatory networks in shaping the shared phenotypic variability across different perturbations.

Introduction

The rate and direction of phenotypic evolution depend not only on natural selection but also on the availability of phenotypic variants, whether induced genetically or environmentally, upon which selection may act[1]. Even environmentally induced phenotypic variability or plasticity has the potential to initiate and direct adaptive evolution through processes such as genetic assimilation[2]. It is widely acknowledged that organisms exhibit heterogeneous phenotypic variation, with certain variants emerging more frequently than others in response to genetic or environmental perturbations[3, 4, 5, 6]. This bias in phenotypic variability can facilitate and constrain adaptive evolution across different phenotypic dimensions[7], contingent on the alignment between the bias in phenotypic variability and the direction of selection[8]. Thus, without a thorough understanding of the nature of phenotypic variability, our understanding of why evolution has progressed in the manner that it does or why some phenotypes evolve repeatedly while others are one-offs remains incomplete.

Seemingly different types of phenotypic variability may actually be driven by a common mechanism. Theoretical studies have demonstrated that the bias in phenotypic variability is shared by different perturbations[9, 10, 11, 12, 13, 14]. Notably, several quantitative genetic studies identified similarity in the magnitude of variance, where traits sensitive to environmental perturbations tend to be sensitive to genetic perturbations[15, 16, 17, 18]. Additionally, there is a consistent pattern of directional variation among traits, with organisms frequently exhibiting correlated variation between traits[19]. Environmental influences on traits often act in the same direction as genetic influences, thereby shaping phenotypic variation in a consistent direction[6]. These similarities imply the existence of a common mechanism underlying the bias in phenotypic variability against any kinds of perturbations[12, 13, 14, 20, 21].

What molecular mechanisms bias the phenotypic variability? In biological systems, most traits arise from genetic interactions within networks represented by gene regulatory networks[22]. Genetic and environmental perturbations exert phenotypic effects via identical regulatory networks[23]. Consequently, phenotypic variance is expected to be influenced by the properties of the regulatory networks, regardless of the underlying causes of perturbations[8, 10]. Despite a growing number of studies demonstrating empirical evidence supporting the similarity both in susceptibility and in directionality of variations in gene expression levels between environmental and genetic perturbations[17, 18, 24], it remains largely unknown how the real regulatory networks account for the observed bias in variability among genes[8].

To address this issue, we characterize the variability of transcriptome profiles in *Escherichia coli* in response to different environmental and genetic perturbations. *E. coli* is an ideal model organism for this investigation because of its well-characterized gene regulatory network. Our analysis reveals that genes showing higher transcriptional variability against environmental perturbations tend to have higher sensitivity to genetic perturbations, indicating a shared gene-to-gene bias in variability across different types of perturbations. In addition, the major directions, or the top principal components, of

correlated variation among thousands of genes are shared by different perturbations, demonstrating a common bias in the directionality of transcriptional changes. We identify 13 global transcriptional regulators that underlie this shared transcriptional variability across various perturbations. Genes regulated by these key regulators tend to exhibit greater transcriptional variability compared to those regulated by other transcriptional regulators. Moreover, these global regulators orchestrate coordinated transcriptional changes in their target genes, contributing to the predominant directionality of transcriptomic shifts observed across different perturbations. These empirical findings support the relevance of the gene regulatory networks in explaining the bias in phenotypic variability shared across different perturbations. Our results suggest that these biases are not random but are functionally significant in coping with fluctuating environments.

Results & Discussion

Similarity in transcriptional variance between environmental and genetic perturbations

We initially analyzed two public transcriptome datasets to evaluate the transcriptional variability across different perturbations. To this end, we curated transcriptome profiles from the PRECISE database[25, 26], focusing on a single strain of *E. coli*, K12 MG1655, cultured under different environmental conditions (160 profiles, 76 unique environmental conditions) (**Supplementary Data 1, Supplementary Fig. 1a,b**), termed the Env dataset (**Fig. 1a**). Additionally, to evaluate transcriptional variability in response to genetic perturbations via natural evolution, we used transcriptome profiles from 16 natural strains of *E. coli* cultured under an identical environmental condition[27], termed the Evo dataset (**Fig. 1b**). These isolates spanned the most common phylogroups and lifestyles of *E. coli*. Importantly, genetic mutations among these strains might reflect their diverse natural habitats, potentially confounding the estimation of transcriptional variability in response to genetic perturbations independent of environmental perturbations. To mitigate this, we conducted a mutation accumulation (MA) experiment[28] using a mutator strain of *E. coli*, K12 MG1655, lacking the *dnaQ* gene[29, 30] (**Fig. 1c**). Here, mutations primarily accumulate through genetic drift owing to small population bottlenecks, thus minimizing positive selection. We established two founder colonies (founders A and B) and propagated single colonies on lysogeny broth (LB) agar plates (yielding three MA lineages per founder). Consequently, we obtained transcriptome profiles from six MA lineages cultured in LB broth using the reliable DNA microarray technique[31] (**Supplementary Fig. 1c,d**), termed the Mut dataset (**Supplementary Data 2**,**3**). Importantly, each dataset was generated within single laboratories using a common protocol, minimizing technical variation within each dataset. We used quantile-normalized and $\log_2$-transformed transcriptome data for the analysis.

The means and standard deviations of expression levels were computed for each gene across each dataset (**Fig. 1d** for six representative genes). While standard deviation might directly measure transcriptional variability, it can be influenced by the mean[32], leading to a confounding effect in estimating similarities in transcriptional variability between datasets. Notably, the standard deviations exhibited a statistically significant mean dependency for all datasets (**Fig. 1e**). To alleviate this influence, we calculated the vertical deviation of each standard deviation from a smoothed spline of the running median of the standard deviations (DM), which served as a measure of the magnitude of transcriptional variability. The DM values of each gene in the dataset was designated as DM_{env}, DM_{evo}, DM_{mut} for the Env, Evo, and Mut datasets, respectively (**Fig. 1f**, **Supplementary Data 4**).

Since each transcriptome profile for all datasets was obtained from millions of cells in unsynchronized cultures, gene expression levels are expected to be independent of the well-known temporal fluctuations in expression associated with the cell cycle. Unlike animals and plants, *E. coli* lacks developmental stages, and its temporal fluctuations in gene expression are primarily linked to replication-dependent changes in gene dosage [33]. To verify that cell-cycle fluctuations did not confound our results, we examined the relationship between known temporal variability in mRNA expression

and DM values. Pountain et al. performed single-cell RNA sequencing on the *E. coli* K12 MG1655 strain and quantified cell-cycle-dependent changes in gene expression. The amplitude of these fluctuations was measured as the fold change from trough to peak in mRNA levels within a cell cycle. Larger amplitudes represent higher temporal variability in mRNA expression without environmental or genetic perturbations. We confirmed that there was no positive correlation between DM values and the amplitude of cell cycle expression (**Supplementary Fig. 2a**). This is consistent with the expectation that our transcriptomic profiles reflect the population averages of unsynchronized *E. coli* cultures, and thus DM values did not reflect cell-cycle-associated temporal fluctuations.

In principle, replication-dependent changes in gene dosage could still influence DM values, even in unsynchronized cultures. At higher growth rates, overlapping cycles of replication occur, leading to higher copy numbers of genes located near the origin of replication (*oriC*). In slower growth conditions, this overlap does not occur, making gene dosage near *oriC* more sensitive to growth rate changes. This could potentially increase the transcriptional variability of genes near *oriC* across different environmental or genetic conditions. To test this, we explored the relationship between DM values and the genomic distance from *oriC* (**Supplementary Fig. 2b**). We found no significant negative correlation, suggesting that replication-dependent gene dosage effects did not significantly confound the DM values.

In addition to using unsynchronized cultures, we also accounted for the growth phase of the cultures in the Mut and Evo datasets. A previous study confirmed that transcriptome profiles obtained at different time points during the exponential growth phase under identical conditions are highly similar, especially when compared to profiles obtained under different environmental conditions or during other growth phases [34]. To minimize the risk of unknown temporal fluctuations in expression levels in the absence of environmental changes, we performed transcriptomics on populations of exponentially growing cells under identical conditions for both the Mut and Evo datasets. Ideally, sampling the same cells multiple times under the same conditions could further validate these assumptions. However, both RNA sequencing and the microarray techniques used in this study are invasive methods for measuring gene expression, making this approach impractical. Unlike the other datasets, the Env dataset involved different growth conditions, and sampling times varied depending on the environment, meaning that some samples were taken outside the exponential growth phase. To assess the impact of these profiles on DM_{env}, we extracted the transcriptome profiles from the exponential growth phase within the Env dataset to construct a refined dataset, termed Envexp, based on information from the original papers in the PRECISE database. Recalculating DM values (DM_{envexp}) from this dataset (78 profiles, 37 unique environmental conditions, **Supplementary Data 1**), we observed a high correlation between DM_{env} and DM_{envexp} (**Supplementary Fig. 3**). Additionally, we confirmed that DM_{envexp} positively correlated with DM_{evo} and DM_{mut}, with correlation levels nearly equivalent to those of DM_{env} (**Fig. 2a**). These results indicate that samples taken outside the exponential growth phase did not significantly affect DM_{env}. Thus, we conclude that DM_{env} primarily

153 reflects transcriptional changes in response to environmental perturbations, rather than temporal
154 changes independent of environmental conditions. Overall, DM values are reasonably assumed to
155 reflect transcriptional changes in response to environmental or genetic perturbations, rather than
156 temporal fluctuations without such perturbations.

157 Comparing DM values between datasets revealed positive correlations (Spearman's rank
158 correlation coefficient (R) =0.43–0.56, $p<0.05$) (**Fig. 2a**). These results indicate that genes with higher
159 sensitivity to environmental perturbations tend to have higher sensitivity to genetic perturbations in
160 terms of their expression levels. This phenomenon of canalization/decanalization could occur not only
161 at the gene level but also at more complex phenotypes subject to natural selection.
162 Canalization/decanalization in transcriptional changes has been observed in some functional categories
163 of genes in yeast[18, 24]. For instance, genes involved in stress or amino acid metabolism tend to have
164 higher transcriptional variability [24], while genes related to cell growth, maintenance, and cell cycles
165 tend to have lower transcriptional variability against genetic perturbations, compared to random
166 expectations [18]. To explore whether functional associations in DM values were present in bacteria, we
167 utilized a refined subset of Gene Ontology (GO) terms as functional categories (**Methods**)
168 **(Supplementary Data 5**). Using the mean DM values of genes within each GO term as a measure of
169 transcriptional variability, we observed positive correlations between the datasets even at the functional
170 category level (**Fig. 2b**). To further investigate functional associations in DM values, we performed
171 gene set enrichment analysis (GSEA[35]) with GO terms for both higher and lower DM values for each
172 dataset independently. We found several GO terms significantly enriched in higher or lower DM values
173 (BH-adjusted p-value (q)<0.05, GSEA). For instance, we identified genes related to 13 GOs that were
174 significantly overrepresented at higher DM values compared with a uniform distribution. We identified
175 several common GO terms across all datasets (**Fig. 2c**, **Supplementary Fig. 4**). For higher DM values,
176 more than three GOs were found at every intersection between pairs of datasets. This overlap was
177 significantly more than expected ($p<0.0001$) based on random drawing from a pool of 81 GOs without
178 replacement. Notably, genes related to flagellum-dependent cell motility and amino acid catabolic
179 processes were consistently enriched with higher DM values in all three datasets (q<0.05, GSEA).
180 Tuning the activity of these functional categories in response to environmental changes is crucial for
181 cells to cope with nutritionally fluctuating environments[36, 37]. In contrast, genes related to fundamental
182 biological processes related to cell-wall construction and maintenance were consistently enriched at
183 lower DM values for all datasets (q<0.05, GSEA, **Fig. 2c right**), indicating that the expression levels
184 of genes within these categories were relatively robust to perturbations. The number of these common
185 GOs (7) in lower DM values was significantly larger ($p<0.0001$) than expected (0.06) based on random
186 drawing from a pool of GOs without replacement. We obtained relevant results using the functional
187 categories defined by the KEGG pathways (**Supplementary Fig. 5**,**6**, **Supplementary Data 6**). There
188 were positive correlations in DM values at the pathway level between the three datasets (Spearman's
189 R=0.5–0.67, $p<0.05$). Additionally, genes related to chemotaxes and peptidoglycan biosynthesis were
190 overrepresented at higher and lower DM values, respectively, for all datasets (q<0.05, GSEA). These

191 KEGG pathways were closely related to flagellum-dependent cell motility and cell-wall construction
192 in GO terms, respectively. These results indicate frequent associations between
193 canalization/decanalization in transcription level of genes and their functions, suggesting a certain
194 common mechanism underlying the heterogeneous transcriptional variability associated with
195 functional categories.

196 **Transcriptional regulators influencing transcriptional variability**

197 To explore the underlying mechanism, we examined the influence of transcriptional regulators on
198 transcriptional variability. First, we conducted GSEA for each dataset independently based on known
199 regulatory interactions (**Supplementary Data 7**) to identify transcriptional regulators that affect target
200 genes exhibiting higher and lower DM values, termed TR_{high} and TR_{low}, respectively. We analyzed two
201 golden standard databases, RegulonDB[38] and EcoCyc[39], collecting known regulatory interactions
202 between genes. We focused on the transcription factors and sigma factors that regulate more than four
203 and less than 1001 target genes. For the Env dataset, we identified 30 transcriptional regulators
204 enriched in higher DM_{env}, such as FlhDC and Fur, and termed them TR_{env} ($q<0.05$, GSEA, **Fig. 3a**).
205 This enrichment means that the target genes of these regulators were overrepresented at higher DM_{env}
206 compared with a uniform distribution. In contrast, we identified only four transcriptional regulators
207 enriched in the lower DM_{env} ($q<0.05$, GSEA). Similar analyses were performed for DM_{evo} and DM_{mut},
208 independently (**Supplementary Fig. 7**). Consequently, we identified 29 (TR_{evo}) and three
209 transcriptional regulators enriched in higher and lower DM_{evo}, respectively. Similarly, 28 (TR_{mut}) and
210 two transcriptional regulators were enriched in the higher and lower DM_{mut}, respectively ($q<0.05$,
211 GSEA). Thus, fewer transcriptional regulators were overrepresented at lower DM values, suggesting
212 that regulation by transcriptional regulators tends to increase the transcriptional variability of target
213 genes, with some regulatory motifs, such as negative feedback, potentially repressing fluctuations in
214 gene expression, as a minor exception[40].

215 Next, we explored the similarity between TR_{env}, TR_{evo}, and TR_{mut}, which were identified in
216 each dataset independently. We found that 13 transcriptional regulators, referred to as TR_{com}, were
217 common among the three datasets, corresponding to more than one-third of the transcriptional
218 regulators enriched in each dataset (**Fig. 3b**). The number of TR_{com}s (13) was significantly larger
219 ($p<0.0001$) than the expected number (1.7) for the intersection of the three sets, constructed by random
220 drawing from a pool of 118 TRs without replacement. These results suggest that the target genes
221 regulated by TR_{com} exhibited higher transcriptional variability in response to both environmental and
222 genetic perturbations, indicating that TR_{com}s function as a common mechanism to bias transcriptional
223 variability against various perturbations.

224 **Network signatures of transcriptional regulators influencing transcriptional variability**

225 How do TR_{com}s enhance transcriptional variability of target genes against a variety of perturbations
226 both inside and outside of the cells? We found that TR_{com}s are global regulators with a large number
227 of target genes, including TR_{com}s themselves (**Fig. 3c**). Based on these findings, we speculated that

228 TR_{com}s might regulate each other frequently, which could increase the probability of the propagation
229 of different perturbations to their target genes. To test this hypothesis, we explored the regulatory
230 structure of a network comprising TR_{com}s alone (**Fig. 3d**). We found that most TR_{com}s had both an in-
231 degree and an out-degree (11 out of 13 regulators). FliA had no out-degrees but four in-degrees. Only
232 IscR was isolated with no regulatory interactions within TR_{com}s. This network structure indicates that
233 the network within TR_{com}s is not top-down structured but has many mutual interactions (activations
234 and inhibitions) within TR_{com}s. The edge density within the TR_{com}s (**Fig. 3e**) was remarkably high
235 (0.17), with statistical significance ($p<0.0001$), compared to the edge density of random expectations
236 (0.019). These results indicate that the TR_{com}s form a relatively densely connected network that is
237 proficient in propagating the influence of perturbations within this group.

238 Next, we explored the effects of TR_{com}s on transcriptional variability. First, we compared the
239 DM values of the target genes with TR_{com}-containing regulation with those of the target genes with
240 TR_{com}-less regulation (**Fig. 4a**). The target genes of TR_{com}s tended to have higher DM values in all
241 datasets than other genes with the same number of unique regulators. We found none or very weak
242 positive correlations between the DM values of the genes without regulations by TR_{com}s and the
243 number of unique regulators that the genes received in all datasets (Spearman's R=~0.13). On the other
244 hand, the target genes of TR_{com}s exhibited relatively high positive correlations in all datasets
245 (Spearman's R=0.23–0.35, $p<0.05$). These results indicate that the recruitment of TR_{com}s is more
246 effective in enhancing transcriptional variability. To further investigate this hypothesis, we explored
247 the relationship between DM values and the number of unique TR_{com}s among the genes with a fixed
248 number of regulators. In the case of the genes that received five unique regulators (**Fig. 4b**), we found
249 a positive correlation between DM_{env} and the number of unique TR_{com}s among the five regulators
250 (Spearman's R=0.29, $p<0.05$). We performed similar analyses for all the datasets and found pervasive
251 positive correlations across broad classes of the number of unique regulators (**Fig. 4c**). These results
252 highlight the role of TR_{com}s in enhancing transcriptional variability through dense mutual regulation
253 within TR_{com}s and co-regulation by multiple TR_{com}s, likely because both increase *trans*-target sizes[18]
254 that affect the expression levels of the genes regulated by TR_{com}s in response to both environmental
255 and genetic perturbations.

256 To understand how TR_{com}s access a variety of perturbations, we explored the relationship
257 between TR_{com}s and the known molecular machinery for sensing stimuli both inside and outside the
258 cells. First, we performed bow-tie decomposition of the TRN to identify the subnetworks to which the
259 TR_{com}s belonged (**Fig. 5a–d**, **Supplementary Data 8**). The *E. coli* TRN was formally dissected into
260 seven sectors defined by Yang's bow-tie structure[41] based on the directed regulatory links between
261 genes[42]. The primary sectors are IN, OUT and the greatest Strongly Connected Component (SCC).
262 The SCC sector represents the subnetwork, in which each node (TR) is reachable by any other node
263 following the direction of regulation from the TR to its target. The IN sector comprises TRs that are
264 not included in the SCC and can reach TRs in the SCC. The OUT sector comprises nodes (TRs or non-

265 regulatory genes) not included in SCC but reachable by TRs in SCC. The numbers of nodes in these
266 primary sectors in *E. coli* TRN were seven TRs, 62 TRs and 2715 genes including the TRs for IN,
267 SCC, and OUT, respectively (**Fig. 5e**). As expected from their many target genes, TR_{com}s (12 of 13
268 TR_{com}s) and TR_{high}s (26 of 48 TR_{high}s in Env, Evo, and Mut) belonged to SCC (**Fig. 5d**). This implies
269 that TR_{com}s can receive broad perturbations from approximately 70 genes in the IN and SCC sectors.
270 We noted that TR_{com}s in SCC still showed a higher edge density (0.19) than other TRs in SCC
271 ($p<0.005$), supporting the especially dense connections within the TR_{com}s.

272 Next, we investigated how TR_{com}s sense different intracellular and extracellular stimuli. *E.*
273 *coli* employs at least 145 sensory regulators to transmit various stimuli to the TRN (**Fig. 5b**,
274 **Supplementary Data 8**). These regulators, termed SRs, change their regulatory activity depending on
275 their interactions with corresponding effectors, as summarized by Martínez-Antonio *et al*[43]. For
276 visualization, we defined the STIMULI block as an aggregated group of the known effectors that
277 interact with SRs, such as nutrients, stressors and metabolites. We found that the IN and SCC sectors
278 contained 39 SRs (27% of the total SRs, **Fig. 5f**), which was reasonable agreement with the random
279 expectation based on the number of TRs in these sectors. Interestingly, more than half of TR_{com}s (8 of
280 13) were SRs. These results indicate that TRs in the SCC sectors, TR_{com}s included, not only serve as
281 intermediate managers in information processing but also play a role in sensing different kinds of
282 stimuli. These characteristics of TR_{com}s, particularly their presence in SCC with many SRs, may enable
283 TR_{com}s to access a variety of stimuli both inside and outside the cells.

284 **Similarity in direction of transcriptional variance between environmental and genetic**
285 **perturbations**

286 Next, we explored the major directions of correlated transcriptional variation among thousands of
287 genes. Theoretically, genetically caused phenotypic variance is expected to be the greatest along the
288 major axis or the principal component of environmentally caused phenotypic variance[10, 12, 13]. To
289 identify such principal components (PC) and test this prediction, we performed principal component
290 analysis (PCA) for each dataset (**Fig. 6a**, **Supplementary Figs. 8–10**). The first three principal
291 components (PC1–3) explained 46%, 53%, and 57% of the total variance in the Env, Evo, and Mut
292 datasets, respectively, indicating their significance as the major axes of transcriptional variation for
293 each dataset. Correlation analysis based on the loadings of these major axes revealed similarities in
294 their directions across the datasets (**Fig. 6b**). We used the absolute values of Spearman's R because of
295 the relative nature of the signs of the principal components. Specifically, PC1 in the Env dataset
296 exhibited relatively strong correlations with PC1 and PC2 in the Evo dataset (Spearman's R = 0.45 and
297 0.41, respectively, $p<0.05$) and with PC1 and PC2 in the Mut dataset (Spearman's R = 0.34 and 0.41,
298 respectively, $p<0.05$). Similarly, PC1 in the Evo dataset showed a relatively strong correlations with
299 PC1–3 in the Env and Mut datasets. These correlations in loadings were much stronger than expected
300 (~0.03 in Spearman's R) based on independent datasets comprising no correlations in expression levels
301 between genes (**Supplementary Fig. 11c**). To validate the high similarity of the PCs between the three

302 datasets more formally, we assessed the extent to which the principal components in the Env dataset
303 explained the transcriptional variance in the other two datasets. Overall, all principal components in
304 the Env dataset explained up to 37% and 39% of the total variance in the Evo and Mut datasets,
305 respectively (**Fig. 6c**). These fractions were much larger than random expectations (~3%,
306 **Supplementary Fig. 11d**). Moreover, the cumulative variance plot displayed a convex upward curve
307 for both the Evo and Mut datasets, as well as Env, which was distinct from a linear-like curve in random
308 expectations (blue line in **Supplementary Fig. 11d**). These findings support the notion that the major
309 directions of transcriptional variation in response to environmental perturbations are considerably
310 similar to those observed in response to genetic perturbations, despite a large number of genes.

311 A directional bias in transcriptional variations is expected to reflect transcriptional
312 regulations[8]. To validate this prediction, we explored the transcriptional regulators that contribute to
313 the major directions. Utilizing the loadings of PC1–3 in each dataset, we conducted GSEA (**Fig. 6d**,**e**).
314 We found the transcriptional regulations enriched in the positive and negative directions of PC1–3 in
315 the Env dataset (**Fig. 6d**). For instance, activation by FadR and FlhDC or inhibition by DksA and PdhR
316 was enriched in the positive direction of PC1. Conversely, activation by RcdA and IscR or inhibition
317 by CecR and MarA was enriched in the negative direction of PC1. We conducted a similar GSEA for
318 the other two datasets (**Supplementary Fig. 12**), identifying 31 regulations common across all three
319 datasets (**Fig. 6e**), including 11 regulations by TR_{coms}, which is consistent with the notion that TR_{com}s
320 are global regulators collectively controlling numerous targets. The number of common regulations
321 (31) was significantly larger ($p<0.0001$) than the expected number (0.2) for the intersection of the three
322 sets constructed by random drawing from a pool of 267 regulations without replacement. Overall, these
323 findings support the idea that the similarity in the direction of transcriptional changes in response to
324 different types of perturbations arises from shared transcriptional regulation. To further confirm the
325 relevance of these findings, we analyzed transcriptome profiles of *E. coli* mutants harboring rewired
326 transcriptional regulations[44] that perturb native transcriptional regulations between major global
327 regulators (**Supplementary Fig. 13**). Each of the rewired strains has a unique shuffled synthetic operon
328 comprising a plasmid copy of the native promoter region of a global regulator ('A') and a plasmid copy
329 of a gene coding for another global regulator ('B'). Accordingly, promoter-mediated transcriptional
330 regulations controlling expression of 'A' are newly connected to 'B' without mutating native
331 chromosomal regulations. Consequently, these rewired strains have new regulatory "links" between
332 randomly selected pairs of global regulators, perturbing native transcriptional regulations between
333 global regulators. The transcriptome profiles of the rewired strains were originally obtained by
334 Baumstark *et al*[45] under identical environmental conditions. Using this dataset, termed the Rwr dataset,
335 we performed PCA and explored how the directionality in transcriptional variance differed from the
336 common directionality shared by the three main datasets (**Supplementary Fig. 13c,d**). We confirmed
337 that the top two PCs in Rwr showed lower correlations (~0.18 at most) with those in the three main
338 datasets, which was very different from the higher correlations between the three main datasets (**Fig.
339 6b**). Relatively higher correlations were found between the third PC in Rwr and the top two PCs in the

three main datasets. Consistently, the PCs defined by the Env dataset explained at most 29% of the variance in the Rwr dataset, which was lower than those of the Mut and Evo datasets (**Supplementary Fig. 13e**). These results indicated that the directionality in transcriptional variation between rewired strains was less similar to the common directionality shared in the other datasets. These results highlighted the importance of regulatory networks between global regulators in major directions in transcriptional variability, supporting the relevance of our findings.

Furthermore, functional enrichment in GO terms was observed in the top three PCs across all three datasets (**Fig. 6f**, **Supplementary Figs. 14–16**). The most major direction in Env (PC1) revealed enrichment of translation, cell division, and cell-wall-related biological processes in one direction (positive sign), and responses to starvation and amino acid catabolic/biosynthetic processes in the opposite direction (negative sign). We termed these opposing functional families growth and starvation families, respectively, because of their close association with cellular growth and starvation states in response to environmental conditions[46]. The correlation between PC1 in Env and PC1 and PC2 in Evo and Mut suggested that approximately half to one-thirds of the functional categories in both families were enriched in these PCs, with opposite directions between the families retained across datasets. Importantly, the mutually opposite directionality observed in these functional families tended to be preserved across different perturbations, suggesting a consistent response pattern at the functional category level (**Fig. 6g**).

Similarity of phenotypic variability across various perturbations

Heterogeneous phenotypic variability is not a random occurrence devoid of biological significance (**Fig. 2c** and **6f,g**), but rather it may result from or be facilitated by the adaptive generalization of past environments[9, 10, 11, 12, 13]. In addition, several studies suggest that evolution tends to produce global canalization that buffers phenotypes against not only genetic and environmental perturbations[12, 13, 21], but also perturbations caused by stochastic molecular noise[47, 48]. These findings imply a similarity in variability in gene expression levels across a broader range of perturbations than previously examined. For instance, genes with higher/lower DM values in Env might also have higher/lower transcriptional variability in response to other environmental perturbations or other nongenetic perturbations (molecular noises) untested in the Env dataset. Similarly, genes with higher/lower DM values in response to random mutations accumulated through genetic drift (Mut) might exhibit higher/lower DM values in response to beneficial mutations accumulated by strong selection in adaptive evolution. To address these possibilities and validate a broader applicability of the findings from the main datasets, we analyzed five additional datasets for *E. coli*, termed Strs_hp, Strs_he, Strs, Prtn, and Noise_ch (**Fig. 7a**, **Supplementary Figs. 17–24**, **Supplementary Note 1**). These datasets include transcriptome or proteome profiles obtained under relatively narrower or more specific conditions than the three main datasets (Env, Evo, and Mut), but under several perturbations absent in the three main datasets, except for Prtn. The Prtn dataset, which contains several environmental conditions similar to those used in Env, was used to test whether the bias in transcriptional variability was retained at the protein level.

The phenotypic variabilities based on these datasets, either at the transcriptional or protein level, were termed DM_{strs_hp}, DM_{strs_he}, DM_{strs}, and DM_{noise_ch} as detailed in **Supplementary Note 1**. In short, DM_{strs_hp} and DM_{prtn} show variability in their expression levels (mRNA for Strs_hp and protein for Prtn) in response to various environmental perturbations. DM_{strs_he} and DM_{strs} represent transcriptional variability in response to genetic mutations accumulated through adaptive laboratory evolution under various stressors. DM_{noise_ch} represents the protein noise of clonal populations under identical environmental and genetic conditions. We found that these DM values were positively correlated with those of the three main datasets (**Fig. 7b**). Notably, the correlations with DM_{env} show relatively strong in all pairs (Spearman's $R = 0.31–0.68$, $p<0.05$). Next, we conducted PCA to identify the directionality of each dataset. To understand the similarity in the major directions across the datasets, we compared PC1–3 of these additional datasets with those of the three main datasets (**Fig. 7c**). Correlation analysis using the loadings of PC1–3 revealed that PC1s of the additional datasets tended to correlate with PC1s or PC2s of the three main datasets. In particular, PC1 in the Env dataset showed the strongest correlation with the PC1s of the additional datasets. Thus, transcriptional variability tended to be retained at the protein level, as shown in the Prtn dataset, suggesting the impact of transcriptional regulation on the variability in phenotypes governed by proteins. The similarity in transcriptional variability with Strs_hp supported the impact of the transcriptional variability identified in the three main datasets on broad environmental conditions. Importantly, the similarity with Strs and Strs_he highlighted the impact of transcriptional variability under relaxed selection (Env or Mut) on the evolutionary diversification in transcriptional phenotypes accompanied by adaptive evolution. Interestingly, the transcriptional variability in response to mutations (Mut) was also coupled with stochastic protein noise (Noise_ch), which was previously reported in yeast [18]. Taken together, these results indicated similar trends in gene-to-gene differences in both the magnitude and major directions of expressional variations across various perturbations, suggesting global canalization/decanalization across different perturbations[12, 13, 14, 21, 47].

Concluding remarks

In this study, we characterized the transcriptional variability of *E. coli* against different perturbations and explored the regulatory commonalities between genetic and environmental perturbations. We identified common global transcriptional regulators that underlie the shared variability across different perturbations. These transcriptional regulators interact relatively densely with each other and strongly connect with many sensory regulators, forming a network structure that is favorable to facilitate the frequency of propagation of various stimuli both inside and outside the cells. In addition, the more regulated genes by these influential regulators showed greater changes in expression effectively. PCA revealed that these global transcriptional regulators simultaneously induced changes in the expression levels of multiple genes and contributed significantly to the formation of major directions of genome-wide changes in expression levels. These results provide implications for the molecular mechanisms behind non-uniform phenotypic variability. The observed transcriptional bias was consistent across

diverse conditions, including adaptive evolution, and was closely related to crucial functions for coping with fluctuating environments, suggesting its pervasive impact on both genetic and nongenetic adaptation to environments.

A major limitation of our study is that it focused solely on the transcriptome regulatory networks of a single strain of *E. coli* (MG1655 including its closely-related strains). Currently, most of the reliable knowledge about transcriptional regulatory networks in *E. coli* is heavily restricted to this model strain. Ideally, gathering comprehensive information on the networks of different strains of *E. coli* or other bacterial species with different configurations of transcriptional regulatory networks would enable us to explore how transcriptional variability depends on their transcriptional regulatory networks. This future exploration would also require many transcriptomic profiles under different environmental conditions for each strain to capture the transcriptional variability unique to each. This extension would further underscore the impact of transcriptional regulatory networks on the magnitude and directionality of transcriptional variability.

429 # Methods

430 **Bacterial strains and media**

431 We constructed a mutator strain of *E. coli* MG1655 by deleting the *dnaQ* gene. Deletion was performed
432 using conventional λ RED recombination[49]. In brief, a kanamycin resistance gene flanked by FLP
433 recognition sites was amplified from *E. coli* BW25113 *ΔmoaA::kan*, a strain of the Keio collection[50],
434 by PCR with chimeric primers containing homology arms for the *dnaQ* region. We used the same
435 chimeric primers as those used to knock out *dnaQ* in a previous study[50]. The PCR fragment was used
436 for lambda RED-mediated homologous recombination with pKD46. The obtained strain after
437 obviating pKD46 was called as MG1655 *ΔdnaQ* and used for the MA experiment. We used YENB
438 broth[51] supplemented with 60 mM arabinose (FUJIFILM Wako, Osaka, Japan, 012-04581) and 50
439 μg/mL ampicillin (FUJIFILM Wako, Osaka, Japan, 012-23303) to prepare electrocompetent cells for
440 λ RED recombination. LB agar plates (Miller, BD Difco, 244620) supplemented with 25 μg/mL
441 kanamycin (FUJIFILM Wako, Osaka, Japan, 115-00342) were used as the selective media after
442 electroporation. We used LB agar and broth for the MA experiments and transcriptome analysis of the
443 mutants, respectively.

444

445 **MA experiments**

446 The MA experiments were performed as previous studies[30]. In brief, we used two independent colonies
447 of MG1655 *ΔdnaQ* as founder strains, founder A and B, to alleviate a potential bias of the mutations
448 before the MA procedure that might affect the accumulated mutations of the descendants during the
449 MA procedures[52]. We initially established six independent lineages for each founder in preparation for
450 extinction during MA experiments. The MA experiments were conducted by transferring randomly
451 chosen single colonies to fresh LB agar plates daily. The plates were incubated at 32 °C. The MA
452 procedure was repeated for 30 times. The MA lineages after the 10th and final rounds were stored at –
453 80 °C. Three randomly selected three MA lineages from each founder were subjected to transcriptome
454 analyses (**Supplementary Data 2**).

455

456 **Transcriptome profiling using microarray technology**

457 The detailed procedure for transcriptome profiling has been described in previous study[31]. All strains
458 obtained by the MA experiments were grown in 200 μL of LB medium in 96-well microplates at 32 °C.
459 The cell density was monitored using a 1420 ARVO microplate reader (PerkinElmer Inc., Waltham,
460 Massachusetts, USA). The cell broth was sampled at the exponential phase, when OD_{600} reached in
461 the 0.072–0.135 range. The cell broth was immediately added to an equal volume of ice-cold ethanol
462 containing 10% (w/v) phenol. The cell pellets were obtained by centrifugation at 20,000 × g at 4 °C
463 for 5 min. Total RNA was extracted using an RNeasy Mini kit with on-column DNase I digestion for
464 15 min (Qiagen, Hilden, Germany) according to the manufacturer's protocol. Purified RNA samples
465 were analyzed for quality control using an Agilent 2100 Bioanalyzer and an RNA 6000 Nano kit
466 (Agilent Technologies). Microarray experiments were performed using a custom-designed Agilent

467 8 × 60 K array for the *E. coli* W3110 strain, comprising 12 probes for each gene. Purified total RNA
468 samples (100 ng) were labeled with Cyanine3 (Cy3) using a Low Input Quick Amp WT labeling kit
469 (One-color; Agilent Technologies). The Cy3-labeled cRNA samples were checked for amount
470 (>825 ng) and specific activity (>15 pmol/μg) using a NanoDrop ND-2000 (Thermo Scientific).
471 Subsequently, the labeled cRNA (600 ng) was fragmented and hybridized to a microarray for 17 h
472 while rotating at 10 rpm at 65 °C in a hybridization oven (Agilent Technologies). The hybridized
473 microarray was washed and scanned according to the manufacturer's instructions. Microarray images
474 were analyzed using Feature Extraction version 10.7.3.1 (Agilent Technologies). Duplicate biological
475 data of the founder strains under the same culture conditions were obtained to confirm technical noise.
476 The compendium of transcriptome data obtained from the MA experiment is called the Mut dataset.
477
478 **Compilation of the TRN in *E. coli***
479 We compiled the reported TRN using all interactions with experimental evidence from RegulonDB
480 11.0[38] and EcoCyc[39] for both transcription factors and sigma factors (**Supplementary Data 7**). For
481 transcription factors, the mode of regulation (activation or repression) was also included. We set the
482 mode of regulation by the sigma factor to activation. When multiple modes were reported for a given
483 regulatory mechanism between a transcription factor and its target gene, they were designated as
484 unknown.
485
486 **Analysis of network architecture of TRN using bow-tie decomposition**
487 First, we analyzed the architecture of TRN in *E. coli* based on bow-tie decomposition[42]. We followed
488 the formal definition of the bow-tie structures proposed by Yang *et al*[41]. Their bow-tie structure has
489 seven sectors. The three main sectors are IN, OUT, and SCC. The SCC sector consists of the largest
490 subnetwork in which each node (gene or transcriptional regulator) is reachable by any other node,
491 following the direction of regulation (activation and/or inhibition). The IN sector represents a group
492 of nodes that are not included in the SCC but can reach nodes in the SCC. The OUT sector represents
493 a group of nodes not included in the SCC that can be reached by the nodes in the SCC. The remaining
494 nodes, other than those in the three main sectors, can be further categorized into TUBES,
495 INTENDRILS, OUTTENDRILS, and OTHERS, according to reachability.

496 To understand how the internal and external perturbations of the cells propagate TRN, we
497 embedded links between the internal/external effectors and TRs, as follows. In addition to the bow-tie
498 structure, we also defined the STIMULI block. The STIMULI block does not consist of a gene or
499 regulator, but consists of intracellular and extracellular effectors, such as nutrients, stressors,
500 metabolites, and stimulating transcriptional regulators by allosteric interactions and so forth. We used
501 the compendium of known links between effectors and TRs collected by Martínez-Antonio *et al*[43].
502 These target regulators are defined as SR. SRs change their regulatory activity depending on whether
503 they bind to effectors. The networks obtained are listed in **Supplementary Data 8**.

Data analysis of the three main datasets (Env, Evo and Mut)

In addition to the Mut dataset, we analyzed two datasets of transcriptome in *E. coli*. To estimate the variability in the expression levels of *E. coli* MG1655 in response to environmental changes, we used an updated version of PRECISE[25, 26], which contains the RNA-seq compendium of *E. coli* MG1655 obtained from a single laboratory using a standardized protocol. In particular, the transcriptome profiles of PRECISE 2.0 were downloaded from iModulonDB[53]. We filtered the transcriptome data of any mutant or evolved strains derived from the MG1655 strain or from other strains to avoid mutational effects on transcriptional variance. Consequently, 160 profiles under 76 unique environmental conditions were used (**Supplementary Data 1**). The environmental conditions were mainly combinations of seven base media (LB, M9, W2, CAMHB, Tris-maleic acid minimal medium, M9 without phosphate, RPMI supplemented with 10% LB), 12 carbon sources (acetate, D-ribose, fructose, galactose, glucarate, gluconate, glucose, glycerol, N-acetylglucosamine, pyruvate, sorbitol, xylose), three nitrogen sources (NH_4Cl, cytosine, glutamine), two electron donors (O_2, KNO_3), three trace elements (aebersold trace element mixture, sauer trace element mixture with or without $MgSO_4$), 35 supplements (cytidine, thiamine, leucine, tyrosine, HCl, lactic acid, adenosine, 2, 2′-dipyridyl, $FeCl_2$, NaCl, paraquat, glutathione, adenine, dibucaine, methionine, salicylate, acetoacetate/LiCl, H_2O_2, LiCl, ceftriaxone, ciprofloxacin, glutamate, glycine, L-tryptophan, meropenem, threonine, trimethoprim-sulfamethoxazole, KCl, phenylalanine, uracil, L-arginine, pyruvate, $CuSO_4$, ethanol, $ZnCl_2$), two temperatures (37 °C, 42 °C), three pHs (5.5, 7, 8.5) and two culture types(batch, chemostat). The filtered compendium was called the Env dataset. To estimate the variability in expression levels during the evolution of *E. coli* in nature, we analyzed the RNA-seq compendium of natural isolates of *E. coli* during growth in the exponential phase in LB broth, where the RNA-seq profiles were obtained in a single laboratory using a common protocol[27]. We analyzed the RNA-seq profiles of 16 natural isolates (MG1655, E1114, HS, H120, E1167, TA447, TA054, E101, TA280, M114, TA249, 41-1Ti9, ROAR8, JJ1886, UT189, S88) that covered all five primary phylogroups of *E. coli* (**Fig. 1b**). The isolates originated from various sources: MG1655 and HS were isolated from *Homo sapiens* feces; TA054, TA447, TA280, M114, TA249, and ROAR8 were isolated from the feces of *Isoodon obesulus*, *Bettongia lesueur*, *Dasyurus viverrinus*, *Burramys parvus*, *Dasyurus hallucatus*, and *Cephalophus sylvicultor*, respectively; H120 and UT189 were isolated from *H. sapiens* urine; 41-1Ti9 was isolated from a *H. sapiens* Crohn's disease patient; JJ1886 was isolated from *H. sapiens* blood; S88 was isolated from *H. sapiens* cerebrospinal fluid; E1114 and E101 were isolated from water; and E1167 was isolated from soil. The sources of these isolates have been previously detailed.[27] The compendium of this dataset was called the Evo dataset.

We used 2622 genes that were common to the three datasets (Env, Evo, and Mut) (**Supplementary Data 3**). For all three datasets, the $\log_2$-transformed gene expression levels were used in subsequent analyses. Expression levels were subsequently quantile-normalized. The means and standard deviations of the expression levels of each gene were calculated for each dataset. For the Mut dataset, we first calculated the means and variances of expression levels among the MA lineages

542 of the final rounds, which were derived from the same founder. Subsequently, we averaged the mean
543 and variance of the MA lineages derived from different founders. We obtained the means and standard
544 deviations of the expression levels of MA lineages that underwent 30 rounds of the MA procedure. We
545 found that the standard deviations were dependent on the mean expression levels for every dataset,
546 which can confer a confounding effect on the correlation analysis between the datasets. To compensate
547 for this dependency, we calculated the vertical distance of each standard deviation from a smoothed
548 running median of standard deviations, referred to as the DM, following the method outlined in a
549 previous study[54, 55]. For each gene, we calculated the DM for each dataset and named it DM_{env}, DM_{evo}
550 and DM_{mut} for the Env, Evo, and Mut datasets, respectively. We also calculated variability at the
551 functional category level based on the DM values. Functional categories were defined by Gene
552 Ontologies (GO)[56, 57]. We constructed a subset (82) of GO by removing redundant GO terms based on
553 semantic similarity among GO terms using the GOSemSim[58], AnnotationDbi[59], rrvgo[60] R packages
554 with default parameters. Alternatively, we used the KEGG pathway database[61]. GO terms and KEGG
555 pathways that consisted of fewer than five genes or more than 300 genes were omitted. The mean DM
556 values among the genes belonging to a given GO term or KEGG pathway were used as a measure of
557 variability at the functional category level **(Supplementary Data 5**,**6**).

558 Gene set enrichment analysis (GSEA)[35] was performed using the clusterProfiler R package[62].
559 We used the refined subset of GO terms and KEGG pathways as functional categories. We filtered out
560 the GO terms and KEGG pathways that consisted of fewer than five genes or more than 300 genes.
561 For GSEA of transcriptional regulators, we also filtered out the transcriptional regulators that regulated
562 fewer than five target genes or more than 1000 genes. The q-values were calculated using the
563 Benjamini-Hochberg (BH) procedure[63]. Transcriptional regulators whose target genes were
564 significantly enriched at higher DM in each dataset were called TR_{env}, TR_{evo} and TR_{mut} for the Env,
565 Evo, and Mut datasets, respectively. The 13 transcriptional regulators present in all three groups were
566 called TR_{com}.

567 The edge density of a given gene set belonging to TRN was calculated as the total number of
568 edges (i.e. regulations) within the gene set divided by the total number of possible edges within the
569 gene set. Self-loops (i.e. autoregulations) were ignored. To compare the edge density within TR_{com}s
570 with that within randomly chosen regulators, we generated 10,000 subsets by drawing the same
571 number of TR_{com}s (i.e. 13) transcriptional regulators at random from a pool of transcriptional regulators.
572 The transcriptional regulators that regulated fewer than five target genes were omitted.

573 PCA was conducted using the prcomp function in R. For the Mut dataset, we used all
574 transcriptional profiles, including isolates at rounds 10 and 30, as well as the founders. In PCA, the *k*-
575 th principal component, PC_k, is represented as a linear combination of loadings *a*, and expression levels
576 *x*, as follows:

577 $$PC_{k,D} = \sum_{i}^{N} a_{k,i,D} x_{i,D} \qquad (1)$$

where D, N and i represent the datasets (ex. Env), total number of genes, and i-th gene, respectively. Correlation analysis was performed for the loadings of the top three PCs, that is, PC1–3 between the datasets. The correlation was evaluated using absolute values of the Spearman's rank correlation coefficients (R), as the signs of the PCs are arbitrary.

Data analysis of the Rwr dataset

The Rwr dataset was derived from transcriptome profiles reported by Baumstark *et al* [45]. In the Rwr dataset, *E. coli* TOP10 (K12) strains, which harbor synthetic shuffled operons [44] (referred to as rewired strains), were cultured under identical environmental conditions. Transcriptome profiles were obtained using the DNA microarray technique (**Supplementary Fig. 13a,b**). A total of 2442 genes, shared across the three main datasets, were extracted. The expression profiles were $\log_2$-transformed and quantile-normalized. To facilitate comparison with the Env dataset, which exhibits high reproducibility, transcriptional profiles that showed relatively low quality (less than 0.95 in mean Spearman's R between biological triplicates) were excluded from the Rwr dataset. The transcriptional profiles were subsequently averaged between the triplicates for each rewired strain. We used a computationally generated random dataset, following a multivariate normal distribution, to confirm that this filtration and averaging process yielded high reliability, comparable to the Env dataset. This filtration resulted in transcriptional profiles of 28 rewired strains (**Supplementary Fig. 13c**).

Data analysis of the other omics datasets (Strs_hp, Strs_he, Strs, Prtn and Noise_ch)

The Strs_hp and Strs_he datasets were obtained from transcriptome profiles reported by Horinouchi *et al*[64]. In Strs_hp, *E. coli* MDS42[65], a derivative of MG1655, was cultured under different stress conditions, and transcriptome profiles were obtained using the DNA microarray technique (**Supplementary Fig. 19a**). The transcriptome profiles obtained from the same stressors used in the Env dataset were removed. Transcriptome profiles for eight stressful conditions (cobalt chloride, sodium carbonate, l-malate, methacrylate, crotonate, methylglyoxal, *n*-butanol and cetylpyridinium chloride) and one stress-free condition (modified M9 medium) were analyzed (**Supplementary Data 9**). Thus, the difference in transcriptome profiles within the obtained dataset, called the Strs_hp dataset, represents transcriptional variability in response to environmental perturbations. For Strs_he, transcriptome profiles were obtained for mutants resistant to each of the different stressors cultured under stressor-free conditions using DNA microarrays (**Supplementary Fig. 19b**). These resistant mutants were obtained through adaptive laboratory evolution experiments using MDS42 as the ancestral strain (**Supplementary Fig. 19c**). We removed the transcriptional profiles obtained from the mutants that experienced the same stressors used in the Env dataset. We analyzed the transcriptional profiles of the mutants obtained under the eight stress conditions described above (**Supplementary Data 9**). Thus, the difference in transcriptional profiles within the resultant dataset, called the Strs_he dataset, reflected the transcriptional variability against genetic mutations accumulated through adaptive evolution. Both datasets contained expression levels of 3741 genes (**Supplementary Fig. 19d**).

615 The Strs dataset was obtained from the transcriptome profiles reported by Maeda and Iwasawa
616 *et al*[31]. In the Strs dataset, the different MDS42 mutants isolated from adaptive laboratory evolution
617 experiments in the presence of different stressors were subjected to DNA microarray analysis
618 (**Supplementary Fig. 22a–c**). The evolutionary experiment was aimed at obtaining resistance mutants
619 against each of the different stressors using MDS42 as an ancestral strain. The transcriptome profiles
620 of the mutant and ancestral strains were obtained under stressor-free conditions, similar to those of
621 Strs_hp. We removed the transcriptome profiles of mutants that evolved under the same stressors used
622 in the Env dataset (example. hydrogen peroxide, meropenem). We analyzed the transcriptional profiles
623 of the mutants obtained under the 47 stress conditions as detailed in **Supplementary Data 10**. Thus,
624 the difference in transcriptome profiles within the obtained dataset, called the Strs dataset, contained
625 transcriptional variability against genetic mutations that accumulated through adaptive evolution.

626 For the Strs_hp, Strs_he and Strs datasets, the mRNA expression levels obtained using DNA
627 microarrays were $\log_2$-transformed and quantile-normalized, similar to the Mut dataset.

628 The Prtn dataset was obtained from proteomic profiles reported by Schmidt *et al*[66]. Proteomic
629 profiles with the growth rate were determined for *E. coli* BW25113 cultured under 22 different
630 environmental conditions (including different carbon sources). The difference in proteomic profiles
631 within the resultant dataset, called the Prtn dataset, represented the proteomic variability (2002
632 proteins) in response to environmental perturbations (**Supplementary Fig. 17**). The absolute
633 abundance of proteins (in copies/cell) was $\log_2$-transformed.

634 For all four datasets (Strs_hp, Strs_he, Strs, and Prtn), the means and standard deviations of
635 the expression levels of each gene were calculated across either the mutant or environment in each
636 dataset (**Supplementary Figs. 17**,**19**,**22**). All datasets showed that the standard deviations depended
637 on the mean expression levels. To compensate for this dependency, we calculated the DM values for
638 each gene as the vertical distance of each standard deviation from a smoothed running median of the
639 standard deviations for each dataset as detailed above. Consequently, we obtained DM_{strs_hp}, DM_{strs_he},
640 DM_{strs} and DM_{prtn} for Strs_hp, Strs_he, Strs, and Prtn, respectively. PCA was performed as described
641 previously (**Supplementary Figs. 18**,**21**,**23**).

642 The Noise_ch dataset was obtained from the cell-to-cell heterogeneity of protein expression
643 levels reported by Taniguchi *et al*[67] (**Supplementary Fig. 24**). Briefly, a library of yellow fluorescent
644 protein (YFP) fusion strains of *E. coli* K12 was cultured under identical conditions, and each
645 chromosomal copy of the gene was labeled with YFP fusion. YFP fluorescence was measured using
646 microscopy at the single-cell level, which yielded the fluorescence distribution for each gene (1018
647 genes). For each gene, the protein noise was defined as the variance divided by the square of the mean,
648 which was identical to the coefficient of variation (CV^2)[67]. Therefore, the protein noise in the
649 Noise_chr dataset represents isogenic cell-to-cell heterogeneity in protein expression levels. It is well
650 known that protein noise is mainly composed of two sources: intrinsic noise dominating lowly

651 expressed proteins and extrinsic noises dominating highly expressed proteins. Owing to the Poisson-
652 like statistical nature of intrinsic noise, the protein noise depends on the mean expression levels of the
653 lowly expressed genes (**Supplementary Fig. 24c**). To compensate for this dependency, we calculated
654 the DM values for each gene as the vertical distance of each protein noise ($\log_{10}$-transformed CV^2)
655 from a smoothed running median of the protein noise; this conventional compensation is widely used
656 for protein noise[54, 68]. Consequently, we obtained DM_{noise_ch}, as a measure of variability against
657 stochastic perturbations (**Supplementary Fig. 24d**). Using the noise limits defined by Taniguchi *et al*.,
658 we determined the expression level at which the intrinsic noise limit was equal to the extrinsic noise
659 limit. Genes with expression levels below this threshold were defined as lowly expressed, whereas
660 those with expression levels beyond this threshold were defined as highly expressed. We compared
661 DM_{noise_ch} with the DM values of the other datasets for lowly and highly expressed genes separately.

662 **Data visualization**

663 All figures were generated in R[69] and the following packages were used. The phylogenetic tree of the
664 16 natural isolates of *E. coli* was visualized using the ape[70] and ggtree[71] packages. Pairwise
665 phylogenetic distances were based on core genome alignments and were obtained from a previous
666 study[27]. Network visualization was performed using the ggraph[72], igraph[73] and tidygraph[74] packages.
667 The Venn diagram was visualized using the ggVenndiagram[75], gplots[76] and venneuler[77] packages.
668 Other illustrative plots were generated using the ggplot2[78] and ggpubr[79] packages.
669

670 **Statistics and reproducibility**

671 Two-sided Spearman's rank correlation coefficients were calculated using the cor.test function in R,
672 specifying the method as Spearman. GSEA was performed with the GSEA function in the
673 clusterProfiler R package. The reproducibility of transcriptome profiles in the Env and Mut datasets
674 was confirmed throught biological replicates (**Supplementary Fig. 1**). No statistical method was used
675 to predetermine sample size.
676

Data availability

All microarray data generated in this study have been deposited in the National Center for Biotechnology Information's Gene Expression Omnibus functional genomics data repository (GEO) under accession number GSE260863 [https://www.ncbi.nlm.nih.gov/geo/query/acc.cgi?acc=GSE260863]. Previously published transcriptome profiles of the Env dataset are available in iModulonDB under accession code PRECISE2.0 [https://imodulondb.org/dataset.html?organism=e_coli&dataset=precise2]. Previously published raw reads in RNA-seq experiments of the Evo dataset are available in ArrayExpress with accession number E-MTAB-9036 [http://www.ebi.ac.uk/arrayexpress/experiments/E-MTAB-9036/], with processed transcriptome profiles available in Rousset *et al.* [27] Previously published raw and processed transcriptome profiles of the Strs_hp, Strs_he datasets are available in GEO under accession number GSE89746 [https://www.ncbi.nlm.nih.gov/geo/query/acc.cgi?acc=GSE89746]. Previously published raw and processed transcriptome profiles of the Strs dataset are available in GEO under accession number GSE137348 [https://www.ncbi.nlm.nih.gov/geo/query/acc.cgi?acc=GSE137348]. Mass spectrometry raw data of the Prtn are available in ProteomeXchange Consortium [http://proteomecentral.proteomexchange.org/] under accession number PXD000498 [https://proteomecentral.proteomexchange.org/cgi/GetDataset?ID=PXD000498], with processed proteome profiles available in Schmidt *et al.* [66] Previously published protein noise data of the Noise_ch dataset are available in Taniguchi et al. [67] Previously published raw reads in scRNA-seq experiments analyzing cell-cycle-dependent changes in gene expression are available in GEO under accession number GSE217715 [https://www.ncbi.nlm.nih.gov/geo/query/acc.cgi?acc=GSE217715], with processed data available in Pountain *et al.* [33]

Code availability

Custom scripts used in the manuscript are available at https://github.com/tsuruubi/Variability_E_coli[80].

References

1. Lynch M, Walsh B. *Genetics and analysis of quantitative traits*. Sinauer Sunderland, MA (1998).

2. Levis NA, Pfennig DW. Evaluating 'Plasticity-First' Evolution in Nature: Key Criteria and Empirical Approaches. *Trends Ecol Evol* **31**, 563-574 (2016).

3. Darwin C. *On the origin of species by means of natural selection, or preservation of favoured races in the struggle for life*. London : John Murray (1859).

4. Waddington CH. *The strategy of the genes*. Routledge (1957).

5. Smith JM*, et al.* Developmental constraints and evolution: a perspective from the Mountain Lake conference on development and evolution. *The Quarterly Review of Biology* **60**, 265-287 (1985).

6. Noble DWA, Radersma R, Uller T. Plastic responses to novel environments are biased towards phenotype dimensions with high additive genetic variation. *Proc Natl Acad Sci U S A* **116**, 13452-13461 (2019).

7. Arnold SJ, Pfrender ME, Jones AG. The adaptive landscape as a conceptual bridge between micro- and macroevolution. *Genetica* **112-113**, 9-32 (2001).

8. Uller T, Moczek AP, Watson RA, Brakefield PM, Laland KN. Developmental Bias and Evolution: A Regulatory Network Perspective. *Genetics* **209**, 949-966 (2018).

9. Parter M, Kashtan N, Alon U. Facilitated variation: how evolution learns from past environments to generalize to new environments. *PLoS Comput Biol* **4**, e1000206 (2008).

10. Draghi JA, Whitlock MC. Phenotypic plasticity facilitates mutational variance, genetic variance, and evolvability along the major axis of environmental variation. *Evolution* **66**, 2891-2902 (2012).

11. Kouvaris K, Clune J, Kounios L, Brede M, Watson RA. How evolution learns to generalise: Using the principles of learning theory to understand the evolution of developmental organisation. *PLoS Comput Biol* **13**, e1005358 (2017).

12. Brun-Usan M, Rago A, Thies C, Uller T, Watson RA. Development and selective grain make

plasticity 'take the lead' in adaptive evolution. *BMC Ecol Evol* **21**, 205 (2021).

13. Milocco L, Uller T. Utilizing developmental dynamics for evolutionary prediction and control. *Proc Natl Acad Sci U S A* **121**, e2320413121 (2024).

14. Brun-Usan M, Zimm R, Uller T. Beyond genotype-phenotype maps: Toward a phenotype-centered perspective on evolution. *Bioessays* **44**, e2100225 (2022).

15. Waddington CH. Genetic assimilation of an acquired character. *Evolution*, 118-126 (1953).

16. Wagner GP, Booth G, Bagheri-Chaichian H. A Population Genetic Theory of Canalization. *Evolution* **51**, 329-347 (1997).

17. Rifkin SA, Houle D, Kim J, White KP. A mutation accumulation assay reveals a broad capacity for rapid evolution of gene expression. *Nature* **438**, 220-223 (2005).

18. Landry CR, Lemos B, Rifkin SA, Dickinson WJ, Hartl DL. Genetic properties influencing the evolvability of gene expression. *Science* **317**, 118-121 (2007).

19. Denver DR, Morris K, Streelman JT, Kim SK, Lynch M, Thomas WK. The transcriptional consequences of mutation and natural selection in *Caenorhabditis elegans*. *Nat Genet* **37**, 544-548 (2005).

20. Cheverud JM. A Comparison of Genetic and Phenotypic Correlations. *Evolution* **42**, 958-968 (1988).

21. Meiklejohn CD, Hartl DL. A single mode of canalization. *Trends in Ecology & Evolution* **17**, 468-473 (2002).

22. Barabasi AL, Oltvai ZN. Network biology: understanding the cell's functional organization. *Nat Rev Genet* **5**, 101-113 (2004).

23. Voordeckers K*, et al.* Identification of a complex genetic network underlying *Saccharomyces cerevisiae* colony morphology. *Mol Microbiol* **86**, 225-239 (2012).

24. Tirosh I, Weinberger A, Carmi M, Barkai N. A genetic signature of interspecies variations in gene expression. *Nat Genet* **38**, 830-834 (2006).

25. Sastry AV, *et al.* The *Escherichia coli* transcriptome mostly consists of independently regulated modules. *Nat Commun* **10**, 5536 (2019).

26. Lamoureux CR, *et al.* A multi-scale expression and regulation knowledge base for *Escherichia coli*. *Nucleic Acids Res* **51**, 10176–10193 (2023).

27. Rousset F, *et al.* The impact of genetic diversity on gene essentiality within the *Escherichia coli* species. *Nat Microbiol* **6**, 301-312 (2021).

28. Halligan DL, Keightley PD. Spontaneous mutation accumulation studies in evolutionary genetics. *Annual Review of Ecology, Evolution, and Systematics* **40**, 151-172 (2009).

29. Fijalkowska IJ, Schaaper RM. Mutants in the Exo I motif of Escherichia coli dnaQ: defective proofreading and inviability due to error catastrophe. *Proc Natl Acad Sci U S A* **93**, 2856-2861 (1996).

30. Tsuru S, *et al.* Genomic confirmation of nutrient-dependent mutability of mutators in *Escherichia coli*. *Genes Cells* **20**, 972-981 (2015).

31. Maeda T, *et al.* High-throughput laboratory evolution reveals evolutionary constraints in *Escherichia coli*. *Nat Commun* **11**, 5970 (2020).

32. Singh GP. Coupling between noise and plasticity in *E. coli*. *G3 (Bethesda)* **3**, 2115-2120 (2013).

33. Pountain AW, *et al.* Transcription-replication interactions reveal bacterial genome regulation. *Nature* **626**, 661-669 (2024).

34. Caglar MU, *et al.* The E. coli molecular phenotype under different growth conditions. *Sci Rep* **7**, 45303 (2017).

35. Subramanian A, *et al.* Gene set enrichment analysis: a knowledge-based approach for interpreting genome-wide expression profiles. *Proc Natl Acad Sci U S A* **102**, 15545-15550 (2005).

36. Honda T, Cremer J, Mancini L, Zhang Z, Pilizota T, Hwa T. Coordination of gene expression with cell size enables *Escherichia coli* to efficiently maintain motility across conditions. *Proc Natl Acad Sci U S A* **119**, e2110342119 (2022).

37. Zampieri M, Horl M, Hotz F, Muller NF, Sauer U. Regulatory mechanisms underlying coordination of amino acid and glucose catabolism in *Escherichia coli*. *Nat Commun* **10**, 3354 (2019).

38. Tierrafria VH*, et al.* RegulonDB 11.0: Comprehensive high-throughput datasets on transcriptional regulation in *Escherichia coli* K-12. *Microb Genom* **8**, mgen000833 (2022).

39. Keseler IM*, et al.* The EcoCyc Database in 2021. *Front Microbiol* **12**, 711077 (2021).

40. Becskei A, Serrano L. Engineering stability in gene networks by autoregulation. *Nature* **405**, 590-593 (2000).

41. Yang R, Zhuhadar L, Nasraoui O. Bow-tie decomposition in directed graphs. In: *14th International Conference on Information Fusion*). IEEE (2011).

42. Ghosh Roy G, He S, Geard N, Verspoor K. Bow-tie architecture of gene regulatory networks in species of varying complexity. *J R Soc Interface* **18**, 20210069 (2021).

43. Martinez-Antonio A, Janga SC, Salgado H, Collado-Vides J. Internal-sensing machinery directs the activity of the regulatory network in *Escherichia coli*. *Trends Microbiol* **14**, 22-27 (2006).

44. Isalan M*, et al.* Evolvability and hierarchy in rewired bacterial gene networks. *Nature* **452**, 840-845 (2008).

45. Baumstark R*, et al.* The propagation of perturbations in rewired bacterial gene networks. *Nat Commun* **6**, 10105 (2015).

46. Shoval O*, et al.* Evolutionary trade-offs, Pareto optimality, and the geometry of phenotype space. *Science* **336**, 1157-1160 (2012).

47. Kaneko K. Relationship among phenotypic plasticity, phenotypic fluctuations, robustness, and evolvability; Waddington's legacy revisited under the spirit of Einstein. *J Biosci* **34**, 529-542 (2009).

48. Furusawa C, Kaneko K. Formation of dominant mode by evolution in biological systems. *Phys Rev E* **97**, 042410 (2018).

855 49. Datsenko KA, Wanner BL. One-step inactivation of chromosomal genes in *Escherichia coli* K-
856 12 using PCR products. *Proc Natl Acad Sci U S A* **97**, 6640-6645 (2000).
857
858 50. Baba T*, et al.* Construction of *Escherichia coli* K-12 in-frame, single-gene knockout mutants:
859 the Keio collection. *Mol Syst Biol* **2**, 2006 0008 (2006).
860
861 51. Sharma RC, Schimke RT. Preparation of electrocompetent *E. coli* using salt-free growth
862 medium. *Biotechniques* **20**, 42-44 (1996).
863
864 52. Niccum BA, Lee H, MohammedIsmail W, Tang H, Foster PL. The Spectrum of Replication
865 Errors in the Absence of Error Correction Assayed Across the Whole Genome of *Escherichia*
866 *coli*. *Genetics* **209**, 1043-1054 (2018).
867
868 53. Rychel K, Decker K, Sastry AV, Phaneuf PV, Poudel S, Palsson BO. iModulonDB: a
869 knowledgebase of microbial transcriptional regulation derived from machine learning. *Nucleic*
870 *Acids Res* **49**, D112-D120 (2021).
871
872 54. Newman JR*, et al.* Single-cell proteomic analysis of *S. cerevisiae* reveals the architecture of
873 biological noise. *Nature* **441**, 840-846 (2006).
874
875 55. Uchida Y, Shigenobu S, Takeda H, Furusawa C, Irie N. Potential contribution of intrinsic
876 developmental stability toward body plan conservation. *BMC Biol* **20**, 82 (2022).
877
878 56. Ashburner M*, et al.* Gene ontology: tool for the unification of biology. The Gene Ontology
879 Consortium. *Nat Genet* **25**, 25-29 (2000).
880
881 57. Gene Ontology Consortium. The Gene Ontology knowledgebase in 2023. *Genetics* **224**,
882 iyad031 (2023).
883
884 58. Yu G, Li F, Qin Y, Bo X, Wu Y, Wang S. GOSemSim: an R package for measuring semantic
885 similarity among GO terms and gene products. *Bioinformatics* **26**, 976-978 (2010).
886
887 59. Pagès H, Carlson M, Falcon S, Li N. AnnotationDbi: Manipulation of SQLite-based
888 annotations in Bioconductor. *R package version 1641*,
889 https://bioconductor.org/packages/AnnotationDbi (2023).
890
891 60. Sayols S. rrvgo: a Bioconductor package for interpreting lists of Gene Ontology terms.
892 *microPublication Biology*, https://doi.org/10.17912/micropub.biology.000811 (2023).

61. Kanehisa M, Goto S. KEGG: kyoto encyclopedia of genes and genomes. *Nucleic Acids Res* **28**, 27-30 (2000).

62. Wu T, *et al.* clusterProfiler 4.0: A universal enrichment tool for interpreting omics data. *Innovation (Camb)* **2**, 100141 (2021).

63. Benjamini Y, Hochberg Y. Controlling the False Discovery Rate: A Practical and Powerful Approach to Multiple Testing. *Journal of the Royal Statistical Society: Series B (Methodological)* **57**, 289-300 (1995).

64. Horinouchi T, *et al.* Prediction of Cross-resistance and Collateral Sensitivity by Gene Expression profiles and Genomic Mutations. *Sci Rep* **7**, 14009 (2017).

65. Posfai G, *et al.* Emergent properties of reduced-genome *Escherichia coli*. *Science* **312**, 1044-1046 (2006).

66. Schmidt A, *et al.* The quantitative and condition-dependent *Escherichia coli* proteome. *Nat Biotechnol* **34**, 104-110 (2016).

67. Taniguchi Y, *et al.* Quantifying *E. coli* proteome and transcriptome with single-molecule sensitivity in single cells. *Science* **329**, 533-538 (2010).

68. Silander OK, *et al.* A genome-wide analysis of promoter-mediated phenotypic noise in *Escherichia coli*. *PLoS Genet* **8**, e1002443 (2012).

69. R Core Team. R: A Language and Environment for Statistical Computing.) (2023).

70. Paradis E, Schliep K. ape 5.0: an environment for modern phylogenetics and evolutionary analyses in R. *Bioinformatics* **35**, 526-528 (2019).

71. Yu G, Smith DK, Zhu H, Guan Y, Lam TT-Y. ggtree: an r package for visualization and annotation of phylogenetic trees with their covariates and other associated data. *Methods in Ecology and Evolution* **8**, 28-36 (2017).

72. Pedersen TL. ggraph: An Implementation of Grammar of Graphics for Graphs and Networks. *R package version 221*, https://CRAN.R-project.org/package=ggraph (2024).

73. Csardi G, Nepusz T. The igraph software. *Complex syst* **1695**, 1-9 (2006).

74. Pedersen TL. tidygraph: A Tidy API for Graph Manipulation. *R package version 131*, https://tidygraph.data-imaginist.com (2024).

75. Gao CH, Yu G, Cai P. ggVennDiagram: An Intuitive, Easy-to-Use, and Highly Customizable R Package to Generate Venn Diagram. *Front Genet* **12**, 706907 (2021).

76. Warnes GR*, et al.* gplots: Various R Programming Tools for Plotting Data. *R package version 3131*, https://CRAN.R-project.org/package=gplot (2024).

77. Wilkinson L. Venn and Euler Diagrams. https://www.rforge.net/venneuler/ (2024).

78. Wickham H. ggplot2: Elegant Graphics for Data Analysis. https://ggplot2.tidyverse.org (2016).

79. Kassambara A. ggpubr: 'ggplot2' Based Publication Ready Plots. *R package version 060*, https://rpkgs.datanovia.com/ggpubr/ (2023).

80. Tsuru S. Genetic properties underlying transcriptional variability across different perturbations. *tsuruubi/Variability_E_coli*, https://doi.org/10.5281/zenodo.14241622 (2024).

Acknowledgements

The authors thank H. Koike for providing technical assistance with the MA experiments. The authors acknowledge H. Kotani for providing technical assistance with the DNA microarray experiments. This work was supported by, the Japan Society for the Promotion of Science (JSPS) KAKENHI (18H02427, 24K21985 to S.T.;17H06389 to C.F. and S.T.; 22K21344 to C.F.) and the Japan Science and Technology Agency (JST) ERATO (JPMJER1902 to S.T. and C.F.).

Author Contributions Statement

S.T.: conceptualization, methodology, investigation, visualization, data curation, formal analysis, validation, writing the original manuscript draft, writing—review & editing, fund acquisition., C.F.: resources, writing—review & editing, fund acquisition.

Competing Interests Statement

The authors declare no competing interests.

969 # Figure Legends

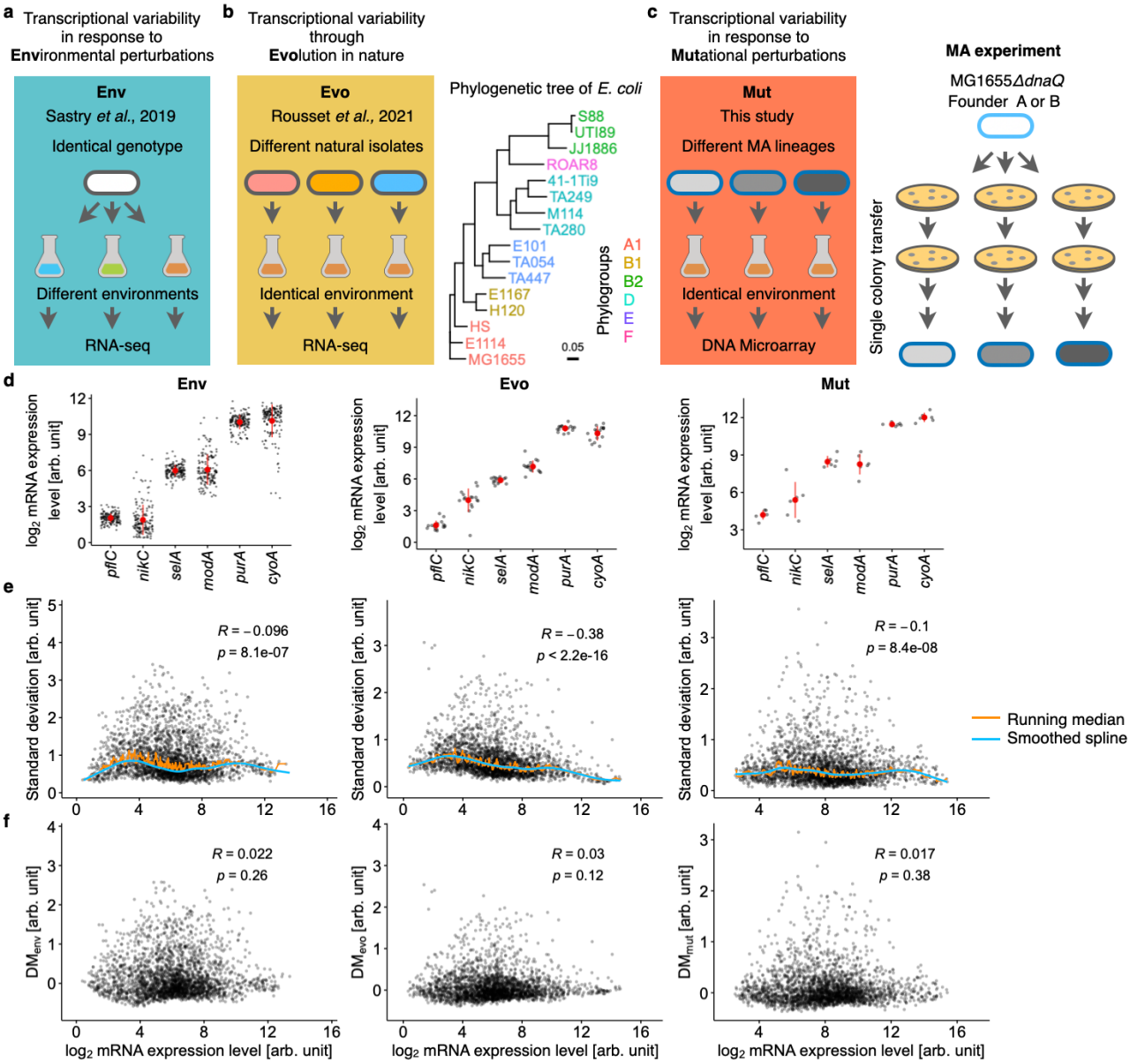

970

971 **Fig. 1: Transcriptional variability in *E. coli*.**

972 **a**, A schematic diagram of the Env dataset. The transcriptome profiles of *E. coli* MG1655 were
973 obtained under various growth conditions[25, 26]. **b**, Schematic of the Evo dataset. The transcriptome
974 profiles of 16 natural isolates of *E. coli* were obtained under a common growth condition[27]. The
975 phylogenetic tree was based on the core genome alignment. **c**, Schematics of the MA and Mut dataset.
976 The MA experiment was initiated by two founders of the mutator strain, *E. coli* MG1655*ΔdnaQ*. Single
977 colonies were randomly picked and transferred daily to fresh LB agar plates for 30 rounds. Three MA
978 lineages from rounds 10 and 30 for each founder were subjected to DNA microarray analysis.
979 Transcriptome profiles were obtained during the exponential growth phase in LB. **d–f**, Transcriptional
980 variability in Env, Evo, and Mut datasets (from left to right). The transcriptome profiles of the MA
981 lineages in the final (30th) round were used for the Mut dataset. **d**, Expression levels of six

representative genes. The expression levels were $\log_2$-transformed and quantile-normalized for each dataset. Each grey circle corresponds to a different bacterial culture. Large closed circles and error bars represent means and standard deviations for the transcriptome profiles of biologically independent samples: Env (n=160 profiles), Evo (n=16 profiles), and Mut (n=6 profiles). **e**, Relationship between means and standard deviations in the expression levels of 2622 genes present in all three datasets. Each dot corresponds to a different gene. The variability metric for each gene was defined as the vertical deviation from a smoothed spline calculated from the running median of the standard deviations. The calculated distance to the median is called DM, with subscripts of the corresponding datasets. For the Mut dataset, the standard deviations were obtained by calculating the variances in expression levels separately in each of the two groups distinguished by the founders (founders A and B) and subsequently averaging them. **f**, Relationship between DMs and mean expression levels. The insets represent Spearman's rank correlation coefficients (R) and p-values (two-sided).

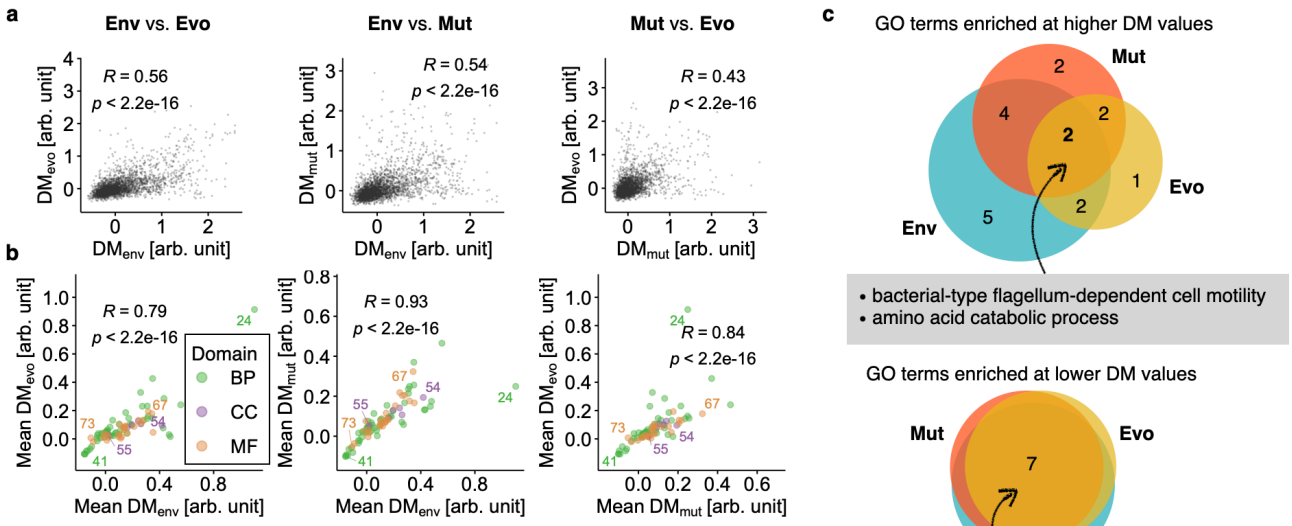

Label	Domain	ID	Term Name
24	BP	GO:0071973	bacterial-type flagellum-dependent cell motility
41	BP	GO:0009273	peptidoglycan-based cell wall biogenesis
54	CC	GO:0055052	ABC transporter complex, substrate-binding subunit-containing
55	CC	GO:0022625	cytosolic large ribosomal subunit
67	MF	GO:0051539	4 iron, 4 sulfur cluster binding
73	MF	GO:0004518	nuclease activity

Fig. 2: Positive correlations of transcriptional variability between datasets.
a, Pairwise correlations are shown for DMs at the gene levels between the Env, Evo, and Mut datasets. **b**, Correlations of DMs at the functional category level between pairs of datasets. The genes were grouped into functional categories based on their GO terms. To reduce the redundancy of GO terms, a custom subset (82) of GO terms was used as detailed in the **Methods** section. Each dot corresponds to a different GO term. The mean DM was calculated by averaging the DM of the genes belonging to each GO term. The three domains of GO–biological processes (BP), cellular components (CC), and molecular functions (MF)–are labeled in different colors. Six representative GO terms are labeled with different numbers, as detailed at the bottom. Spearman's R and p-values (two-sided) are shown in panels **a** and **b**. **c**, Venn diagram of GO terms enriched in higher (left) and lower (right) DM values in each dataset (GSEA, BH-adjusted p-values (q)<0.05, **Supplementary Fig. 4**). The Evo and Mut sets completely overlap in the right Venn diagram. The numbers indicated in the diagram show the number of GO terms enriched in the corresponding set.

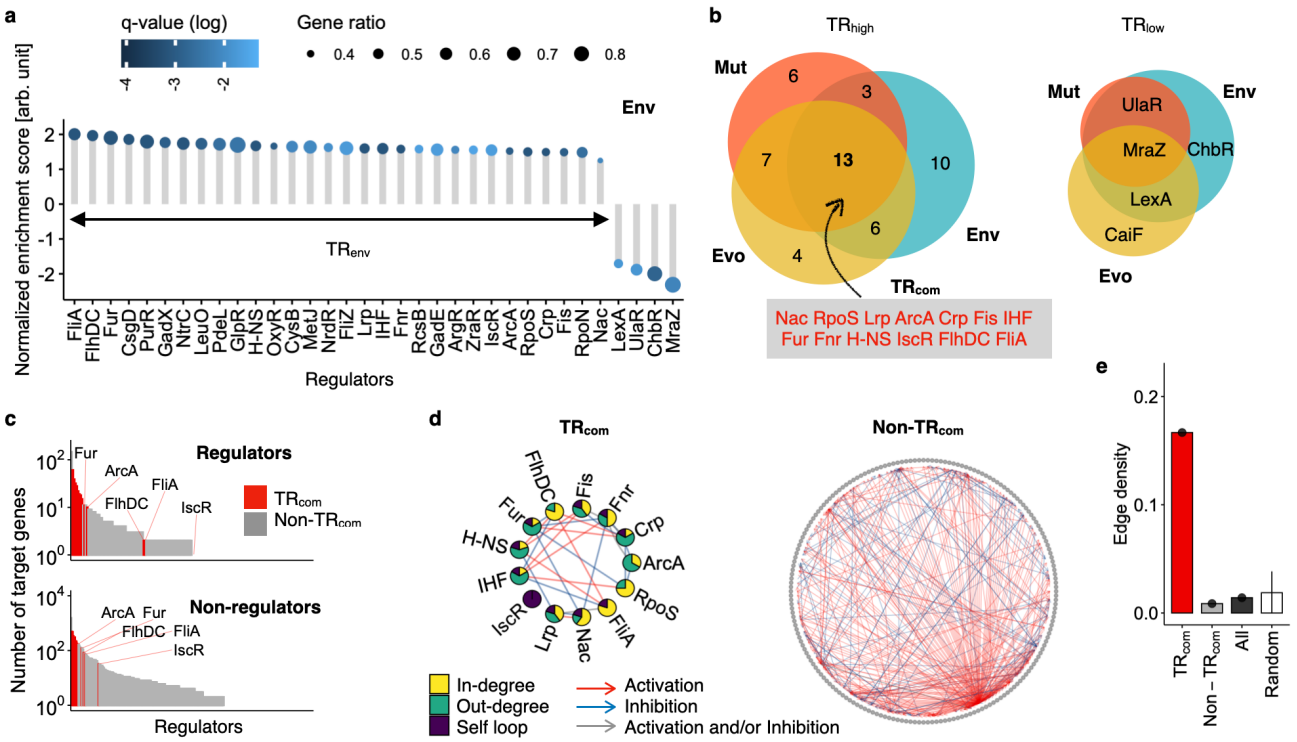

Fig. 3: Transcriptional regulators and transcriptional variability.

a, Transcriptional regulators (TR) enriched in genes with higher and lower DM_{env}. GSEA identified statistically significant TRs ($q<0.05$). Positive and negative enrichment scores indicate enrichment at higher and lower DM_{env}, respectively. The gene ratio was calculated as the number of core target genes contributing to enrichment scores divided by the number of target genes. TRs with positive enrichment scores are labeled as TR_{env}. The q-values (adjusted p-values) were computed using the BH procedure. **b**, Venn diagram of the enriched TRs in each dataset. TR_{evo} and TR_{mut} represent the TRs with positive enrichment scores in the Evo and Mut datasets, respectively. The intersection of the three sets represents TR_{com}. **c**, Rank plot of the number of target genes in the TRs. The TRs were sorted in decreasing order. Target genes were divided into regulators (transcription factors and sigma factors, upper panel) and non-regulators (lower panel). The bars are colored to indicate whether the TRs belong to TR_{com}s or Non-TR_{com}s, with . labels representing subsets of TR_{com}s. **d**, Circular representation of *E. coli* transcriptional regulatory network (TRN) within TR_{com}s (left) and Non-TR_{com}s (right). Edges are colored based on the type of regulation (activation, inhibition, and activation and/or inhibition). Pie charts indicate the percentage of each degree within the TR_{com} nodes. The edges corresponding to the self-loops were omitted from the visualization. **e**, Edge densities within regulatory groups. The random group was generated by drawing 13 TRs at random 10,000 times from a pool of TRs, where TRs that regulate fewer than five target genes were omitted. The bar and error bar for the random group represent the mean and standard deviation (n=10,000), respectively. By definition, the sample size for the other groups was one. Edge density was calculated as the total number of edges within the regulators divided by the total number of possible edges within the regulators, excluding the self-loops.

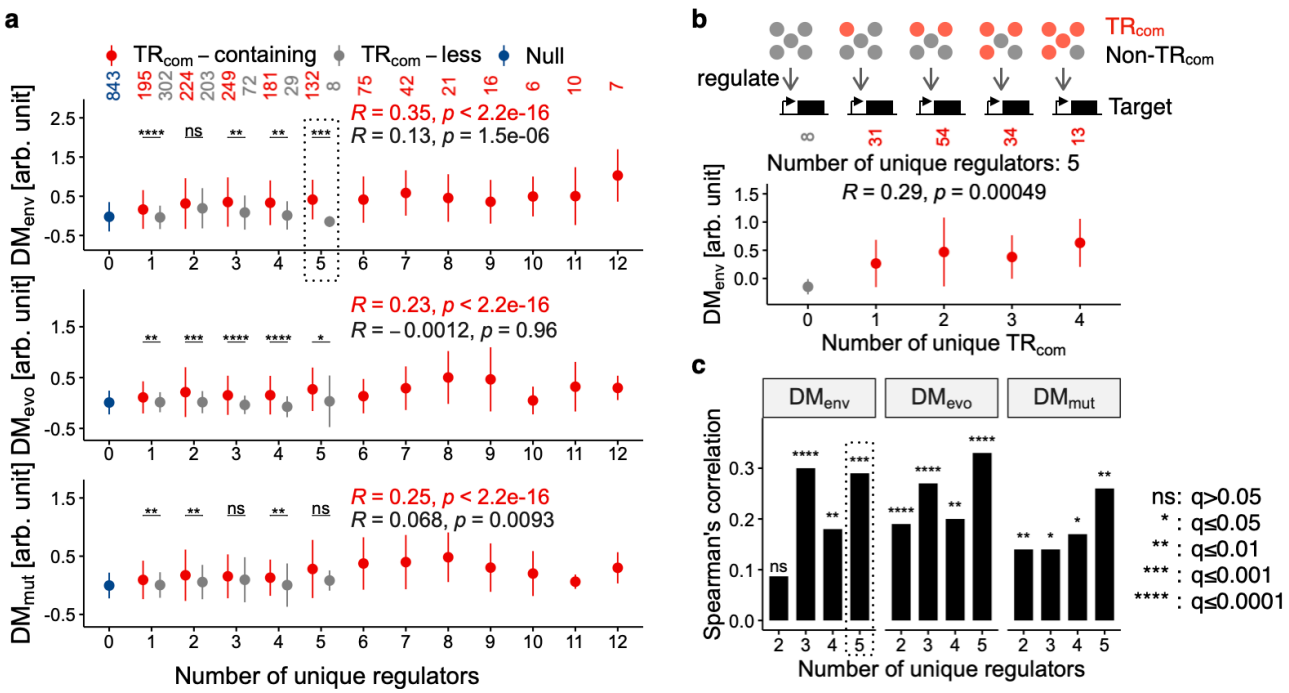

Fig. 4: Relationship between transcriptional variability and the number of transcriptional regulators

a, Relationship between DM values and the number of unique regulators. The top, middle, and bottom panels show the DM_{env}, DM_{evo} and DM_{mut}, respectively. Target genes receiving TR_{com}-containing regulation, TR_{com}-less regulation, and genes without known regulators are labeled in different colors. Means and standard deviations are shown as the points and the error bars, respectively. The sample sizes (n) are indicated at the top. Data points for TR_{com}-containing and TR_{com}-less regulations were restricted to those comprising more than four target genes. Spearman's R and p-values (two-sided) were calculated for data points 0–5 on the x-axis for both TR_{com}-containing and TR_{com}-less regulations. Asterisks represent the statistical significance levels (q-values) of the Wilcoxon test between TR_{com}-containing and TR_{com}-less genes in each class. The target genes within the dotted square are used in panel **b**. **b**,**c**, The correlation between DM values and the number of TR_{com} regulations. **b**, Relationship between DM_{env} and the number of TR_{com}s for target genes regulated by any of the five regulators. Means and standard deviations are shown as the points and the error bars, respectively. The sample sizes (n) are indicated at the top. Spearman's R and p-values (two-sided) are shown. **c**, Spearman's R for DM_{env} (left), DM_{evo} (center), and DM_{mut} (right). The enclosed square corresponds to panel **b**.

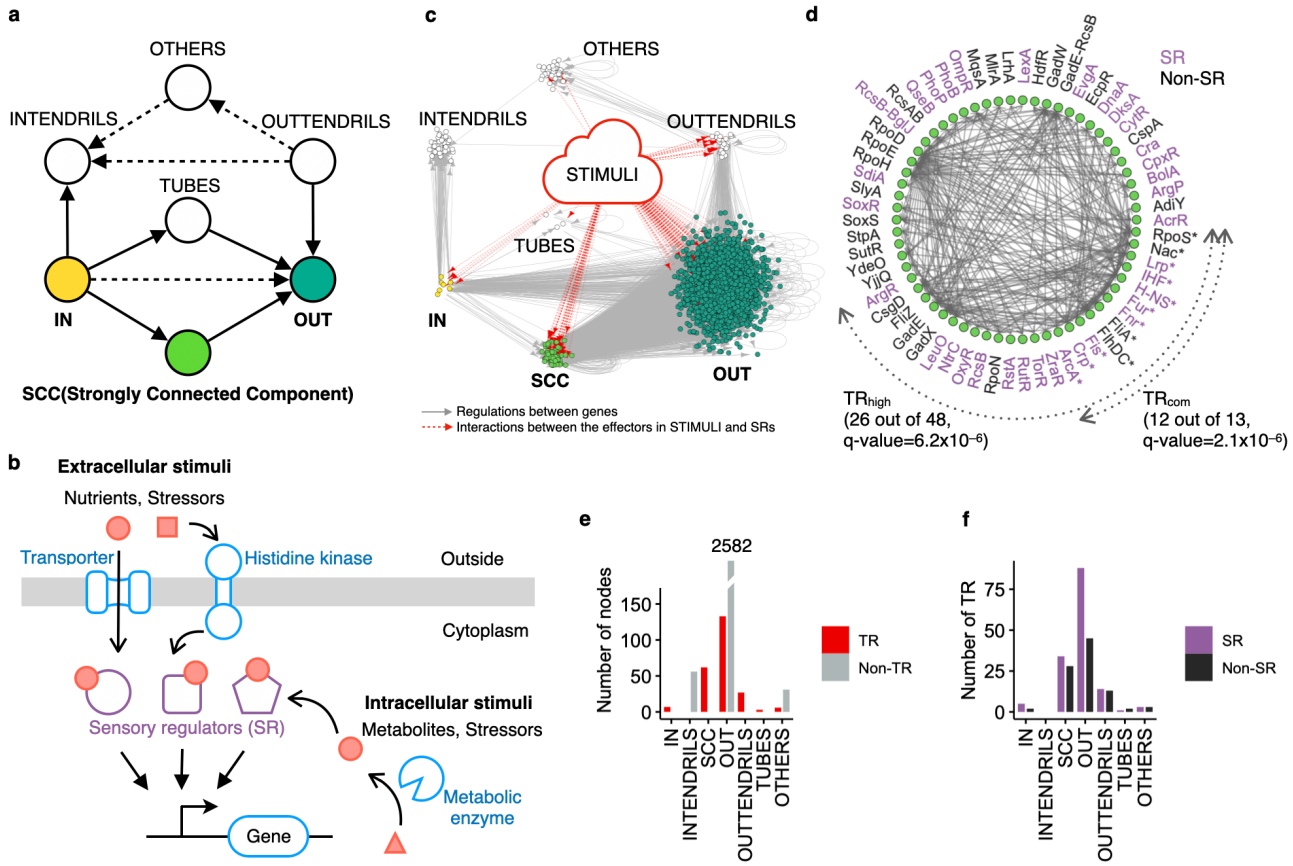

Fig. 5: Bow-tie decomposition of the gene regulatory network in *E. coli*.
a, Yang's bow-tie structure[41] is delineated into seven sectors, with the main sectors highlighted: IN, OUT, and the strongly connected component (SCC). Arrows indicate the direction of regulation, with solid arrows defining each sector and dashed arrows representing possible regulations without violating the sector definitions. **b**, Schematic illustrating how sensory regulators (SR) influence the expression levels of target genes by interacting with intracellular and extracellular effectors (nutrients, metabolites, and stressors). **c**, Bow-tie representation of the gene regulatory network in *E. coli* based on panel **a**. Each node represents a TR or target gene. Solid arrows denote regulation (activation and/or inhibition). The STIMULI block represents an aggregated group of known effectors interacting with SRs, with dotted arrows indicating the interactions between the effectors in STIMULI and SRs. **d**, Regulatory network within the SCC. Each node represents a TR. SR and non-SR groups are labeled in different colors, with asterisks representing TR_{com}. **e**, Distribution of nodes in each sector. TR and non-TR groups are labeled in different colors. IN, SCC, TUBES, and OUTTENDRILS consist solely of TR, whereas INTENDRILS contains only non-TRs by definition. **f**, Number of TR in each sector. SR and non-SR groups are labeled in different colors.

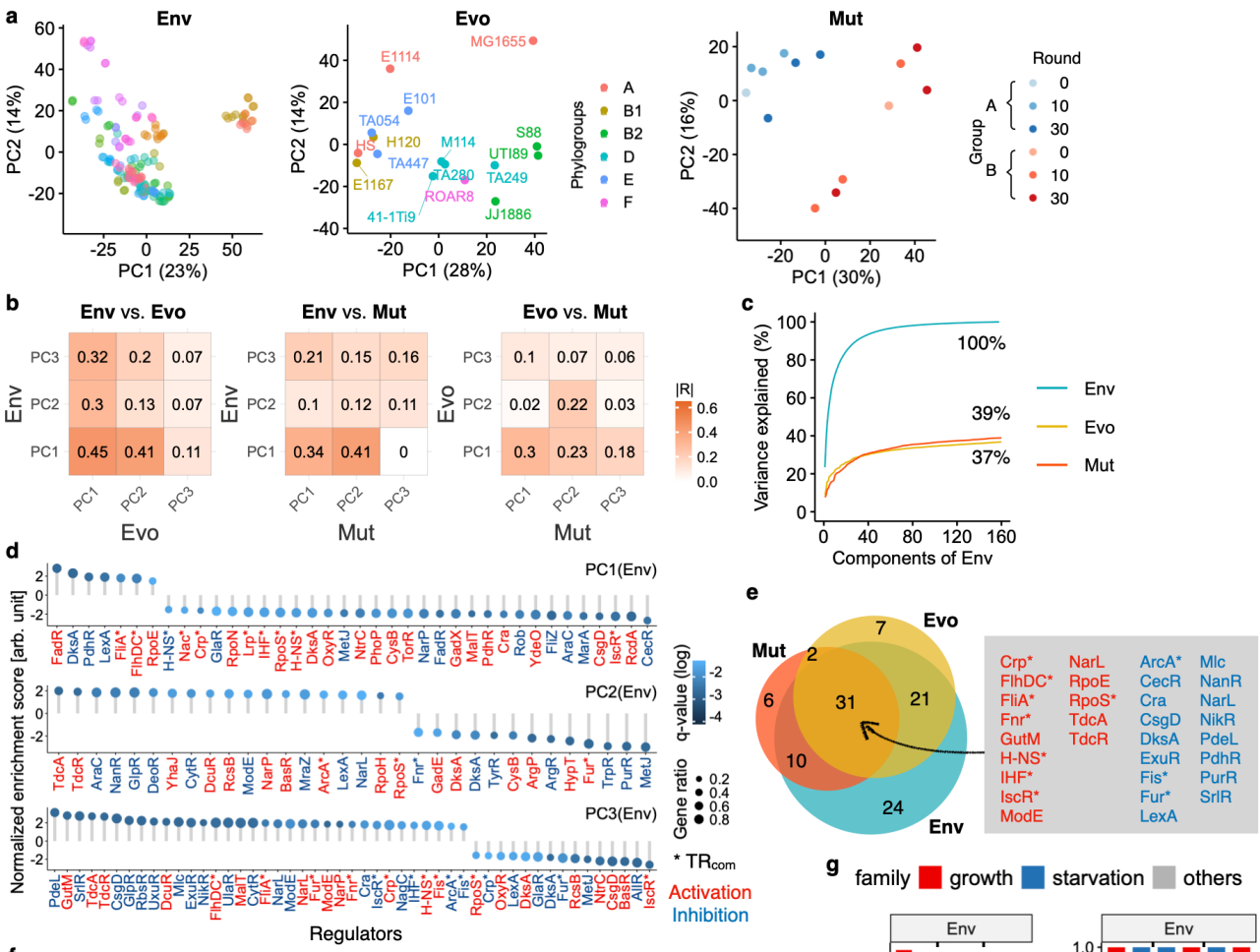

Domain	ID	Term Name
MF	GO:0140640	catalytic activity, acting on a nucleic acid
MF	GO:0003735	structural constituent of ribosome
BP	GO:0006412	translation
BP	GO:0140694	non-membrane-bounded organelle assembly
BP	GO:0001510	RNA methylation

Domain	ID	Term Name
CC	GO:0055052	ABC transporter complex, substrate-binding subunit-containing
BP	GO:0008652	amino acid biosynthetic process
BP	GO:0009401	phosphoenolpyruvate-dependent sugar phosphotransferase system
BP	GO:0006006	glucose metabolic process
BP	GO:0042594	response to starvation

Fig. 6: Alignment of genetic and environmental correlations in transcriptional variability. **a**, First and second principal components (PC) of Env, Evo and Mut arranged from left to right. Points are colored by environmental condition in Env. **b**, Correlation analysis for loadings of the first three PCs among the three datasets. The color scale and numbers in the tiles represent the absolute values of Spearman's R. **c**, Cumulative variance explained by the PCs defined by the Env dataset. Overall, the Env dataset explained 37% and 39% of the variance in the Evo and Mut datasets, respectively. **d**, TRs were significantly enriched (q<0.05) in greater loadings, either positive or negative, of the first three PCs in the Env dataset. GSEA was used to identify regulations, distinguishing between activatory and

inhibitory regulation. Asterisks denote regulations by TR_{com}s. **e**, Venn diagram illustrating the TRs enriched in the first three PCs of each dataset. GSEA was performed for each dataset, as shown in panel **d**. Numbers indicate the number of regulations in the corresponding set. The detailed regulations at the intersection of the three sets are shown on the right. **f**, GO terms enriched with greater loadings in the positive (top) and negative (bottom) directions in PC1 of the Env dataset (five representatives). The former and latter GO terms were categorized into the growth and starvation families. **g**, Number (left) and fraction (right) of GO terms enriched in each sign of each PC in each dataset. GSEA was conducted for each PC in each dataset. The fraction was calculated by dividing the number of GO terms in each family by the total number of GO terms in each PC sign. A full list of the enriched GO terms is presented in **Supplementary Fig. 14–16**.

a

Dataset	Perturbation	mRNA/protein	Variability	Reference
Strs_hp	Environmental	mRNA	DM_{strs_hp}	Horinouchi et al (2017)
Strs_he	Genetic	mRNA	DM_{strs_he}	Horinouchi et al (2017)
Strs	Genetic	mRNA	DM_{strs}	Maeda & Iwasawa et al (2020)
Prtn	Environmental	protein	DM_{prtn}	Schmidt et al (2016)
Noise_ch	Molecular noise	protein	DM_{noise_ch}	Taniguchi et al (2010)

b

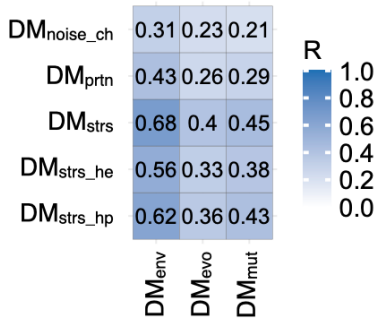

c

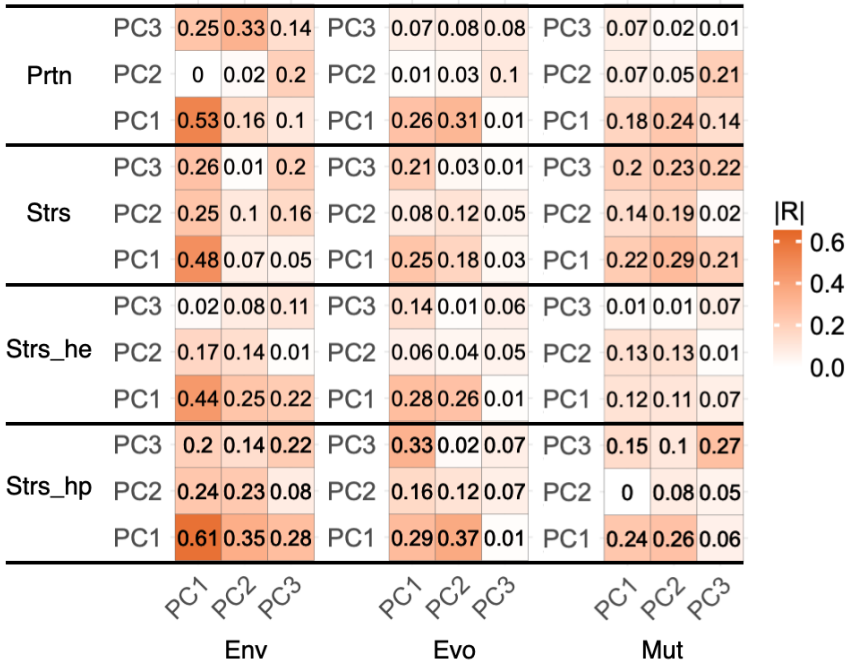

Fig. 7: Similarity of phenotypic variability across different datasets

a, Datasets used to compare similarity in both variability (**b**) and directionality (**c**) of gene expression levels (mRNA/protein) with three main datasets. **b**, Correlation analysis of the variability across different datasets. The color bar and numbers in the tiles represent Spearman's R. Correlation analysis for DM_{noise_ch}, was conducted only for highly expressed proteins with extrinsic noise dominance. The results of the lowly expressed proteins are detailed in **Supplementary Note 1**. **c**, Correlation analysis of loadings of the first three PCs between the datasets. The color bar and numbers in the tiles represent absolute values of Spearman's R.